POLITECNICO DI TORINO
Repository ISTITUZIONALE

Development of a Wearable Sleeve-Based System Combining Polymer Optical Fiber Sensors and an LSTM Network for Estimating Knee Kinematics

Terms of use:

Publisher copyright

(Article begins on next page)

11 March 2025

Development of a Wearable Sleeve-Based System Combining Polymer Optical Fiber Sensors and an LSTM Network for Estimating Knee Kinematics

B. L. Pugliese, *Member, IEEE*, A. Angelucci, *Member, IEEE*, F. Parisi, *Member, IEEE*, S. Sapienza, E. Fabara, G. Corniani, *Member, IEEE*, A. S. Tenforde, A. Aliverti, *Senior Member, IEEE*, D. Demarchi, *Senior Member, IEEE*, and P. Bonato, *Senior Member, IEEE*

Abstract— This study presents a novel wearable solution integrating Polymer Optical Fiber (POF) sensors into a knee sleeve to monitor knee flexion/extension (F/E) patterns during walking. POF sensors offer advantages such as flexibility, light weight, and robustness to electromagnetic interference, making them ideal for wearable applications. However, when one integrates these sensors into a knee sleeve, they exhibit non-linearities, including hysteresis and mode coupling, which complicate signal interpretation. To address this issue, a Long Short-Term Memory (LSTM) network was implemented to model temporal dependencies in sensor output, hence providing accurate knee angle estimates. Data were collected from 31 participants walking at different speeds on a treadmill, using a camera-based motion capture system for validation. Configurations with multiple (up to five) sensors were considered. The best performance was achieved using three sensors, yielding a median root mean square error (RMSE) of 3.41° (interquartile range: 2.50° – 5.19°). Whereas using multiple sensors generally improved robustness, the inclusion of data from sub-optimally placed sensors negatively affected performance. The technology holds potential for clinical application in knee osteoarthritis (OA) management. Future work should focus on optimizing signal calibration and expanding the dataset to facilitate accounting for the different ways in which the knee sleeve conforms to the anatomy of different individuals.

Index Terms— Digital health, kinematics, long short-term memory network, polymer optical fiber sensors, knee osteoarthritis, wearable technology.

B. L. Pugliese is with the Department of Electronics and Telecommunications, Politecnico di Torino, 10129 Turin, Italy, and also with the Department of Physical Medicine and Rehabilitation, Harvard Medical School, Spaulding Rehabilitation Hospital, Boston, MA 02129 USA (e-mail: bpugliese@mgh.harvard.edu).

A. Angelucci and A. Aliverti are with the Dipartimento di Elettronica, Informazione e Bioingegneria, Politecnico di Milano, 20133 Milan, Italy (e-mail: alessandra.angelucci@polimi.it; andrea.aliverti@polimi.it).

F. Parisi, S. Sapienza, E. Fabara, G. Corniani, A. S. Tenforde, and P. Bonato are with the Department of Physical Medicine and Rehabilitation, Harvard Medical School, Spaulding Rehabilitation Hospital, Boston, MA 02129 USA (e-mail: parisi.fed@gmail.com; stefano.sapienza87@gmail.com; efabara@mgb.org; gcorniani@mgh.harvard.edu; atenforde@mgh.harvard.edu; pbonato@mgh.harvard.edu).

D. Demarchi is with the Department of Electronics and Telecommunications, Politecnico di Torino, 10129 Turin, Italy (e-mail: danilo.demarchi@polito.it).

This article has supplementary downloadable material available at https://doi.org/10.1109/TNSRE.2025.3540708, provided by the authors.

Digital Object Identifier 10.1109/TNSRE.2025.3540708

I. Introduction

KNEE osteoarthritis (OA) is a chronic disease of the joint characterized by degenerative changes affecting bone, cartilage, menisci, synovium, and ligaments. This condition affects approximately 9% of men and 18% of women over the age of 65 years [1], [2]. Individuals with knee OA suffer from pain, stiffness, and decreased range of motion (ROM), significantly impairing their physical abilities and restricting daily activities [2], [3]. One of the most prominent gait alterations observed in knee OA patients is reduced knee flexion/extension (F/E) angular displacement during walking, which has been linked to disease progression and symptom severity. Studies have consistently demonstrated that patients with knee OA have significantly lower knee ROM during both the stance and swing phases of gait cycle compared to healthy controls [2], [3], [4], [5]. These altered gait biomechanics may result from joint stiffening and compensatory strategies aimed at minimizing pain and stabilizing the knee. However, such compensation may lead to increased impact loading on the tibiofemoral joint, potentially accelerating disease progression [3], [5].

Despite the potential harm caused by these compensation strategies, maintaining physical activity, particularly through walking programs, is crucial for managing knee OA. Regular movement helps preserve joint function, slow disease progression, and prevent further disability [6], [7], [8]. However, titrating walking programs is challenging. Current methods often rely on self-report of activity, which is not only subjective but also delayed, capturing pain after it has already occurred [9], [10]. This delayed feedback prevents timely adjustments that could help avoid exacerbations.

Real-time monitoring of knee F/E patterns during walking could address this issue by detecting early deviations in movement patterns. By identifying these changes, it may be possible to make proactive adjustments to walking programs, reducing the risk of exacerbating symptoms and preventing disease progression.

Camera-based motion capture systems are considered the gold standard for measuring joint kinematics. However, these systems are expensive, cumbersome, and limited to laboratory environments [11]. Wearable technologies have emerged as a practical solution, offering more accessible ways to track motion in real-world settings [12]. Among them, textile-integrated sensors present a promising avenue for embedding monitoring capabilities into everyday clothing, enabling continuous data collection with minimal burden to the user.

Polymer Optical Fiber (POF) sensors [13], [14], stand out as a particularly suitable option for integration into smart textiles [15]. These sensors offer several advantages over other technologies due to their flexibility, lightweight nature, and robustness to electromagnetic interference. Their flexible nature allows them to conform well to the knee anatomy, enabling unobtrusive data collection during movement. Strategic placement of these sensors at different anatomical locations around the knee captures complementary information, as different sensors are expected to bend differently (according to the anatomical geometry of the knee) during F/E movements. This distributed sensing approach is expected to provide a more accurate estimate of the knee joint angle [16].

POF sensors operate based on the principle of detecting variations in light transmission as the fiber undergoes bending [17]. When light is injected into a POF, it propagates through multiple paths, or modes, within the fiber. These modes are characterized by distinct patterns of internal reflections. Lower-order modes, which involve fewer reflections within the fiber, are marked by minimal attenuation. In contrast, higher-order modes undergo more frequent reflections, leading to signal attenuation as the fiber bends [18]. The multimodal nature of POF sensors causes nonlinearities in the form of mode coupling, where light initially confined to one mode can transfer to another as the fiber bends, thus complicating the interpretation of the sensor's output [19]. Another source of nonlinearity in POF sensors is hysteresis, where the relationship between curvature and light transmission exhibits a lag when the fiber is deformed and returns to its original shape, leading to discrepancies in signal readings depending on the fiber's deformation pattern [20].

To handle the above-described nonlinearities in POF sensor outputs, Long Short-Term Memory (LSTM) networks [21], [22], [23], [24], [25], [26], [27], [28] are employed in this study. LSTMs are designed to analyze timeseries data, allowing them to model temporal relationships. With the integration of redundant sensor data, LSTMs can learn patterns across multiple sensors, providing a robust approach to mitigating individual sensor errors while enhancing the overall precision of the knee angle estimation during walking.

In this study, we utilize a knee sleeve with integrated POF sensors and employ LSTM models to estimate knee F/E angular displacement patterns during walking. We discuss the importance of sensor placement and redundancy in enhancing the system performance. We argue that this work is an important step towards advancing knee OA monitoring, with the ultimate goal of developing effective tools for clinical use.

II. MATERIAL AND METHODS

The experimental setup and the pipeline for data acquisition and processing are shown in Fig. 1. Data were collected from 31 participants walking on a treadmill while wearing the sensorized knee sleeve. Data collected simultaneously via a camera-based motion capture system (Vicon Motion Systems Inc, Oxford, UK) were used as gold standard. The motion capture data were processed and segmented to estimate the patterns of knee F/E angular displacement for each gait cycle. The POF sensors' output was also segmented according to the gait cycles. LSTM networks were trained for various sensor configurations. The performance of the models was evaluated to determine the impact on estimation accuracy of the position of sensors and their number. The error distribution over the gait cycle was derived for the best-performing model.

A. Hardware Description

The knee sleeve, engineered by Mitsui Chemicals (Minato City, Tokyo, Japan), incorporates five multimodal POF sensors, each equipped with an LED at one end and a photodiode at the other. The fibers are encased in a shrink tubing to enhance durability. As the knee undergoes F/E, these fibers deform, altering light transmission and generating voltage variations. The sensors are placed medially (M), laterally (L), inside-medially (IM), inside-laterally (IL), and centrally above the patella (C), as depicted in Fig. 1A. These placements account for the orientation of the Langer's lines [29], [30], [31], [32], [33], with some sensors that align with the Langer's lines and others that are approximately orthogonal to them.

The device is available in three sizes (i.e., medium, large, and extra-large). The voltage output of the sensors ranges between 0 and 5 V. Each sensor is connected via a USB connector to a main board, which is equipped with a dedicated amplification circuit. The circuit consists of a transimpedance amplifier followed by a non-inverting amplifier, with potentiometers in the feedback loop for amplification tuning. To optimize the signal dynamic range, voltage levels are calibrated based on sensor placement and the expected deformation patterns. Channels M, L, and C are set to output approximately 0.5 V when the knee is at 90° of flexion. In contrast, channels IM and IL, which are flexed in the sleeve and extend as the knee flexes, are adjusted to generate an output of 4.5 V when the leg is straight. This setup ensures full use of the voltage range, hence maximizing signal resolution. The amplified signals are then sampled at a rate of 1,800 Hz.

B. Sensor Characterization

A 3D-printed testing rig was developed to characterize the POF sensor output in response to F/E movements. The rig consists of two segments connected by a joint. The POF was positioned in custom housings to ensure smooth bending as shown in Fig. 2. Two reflective markers per segment were
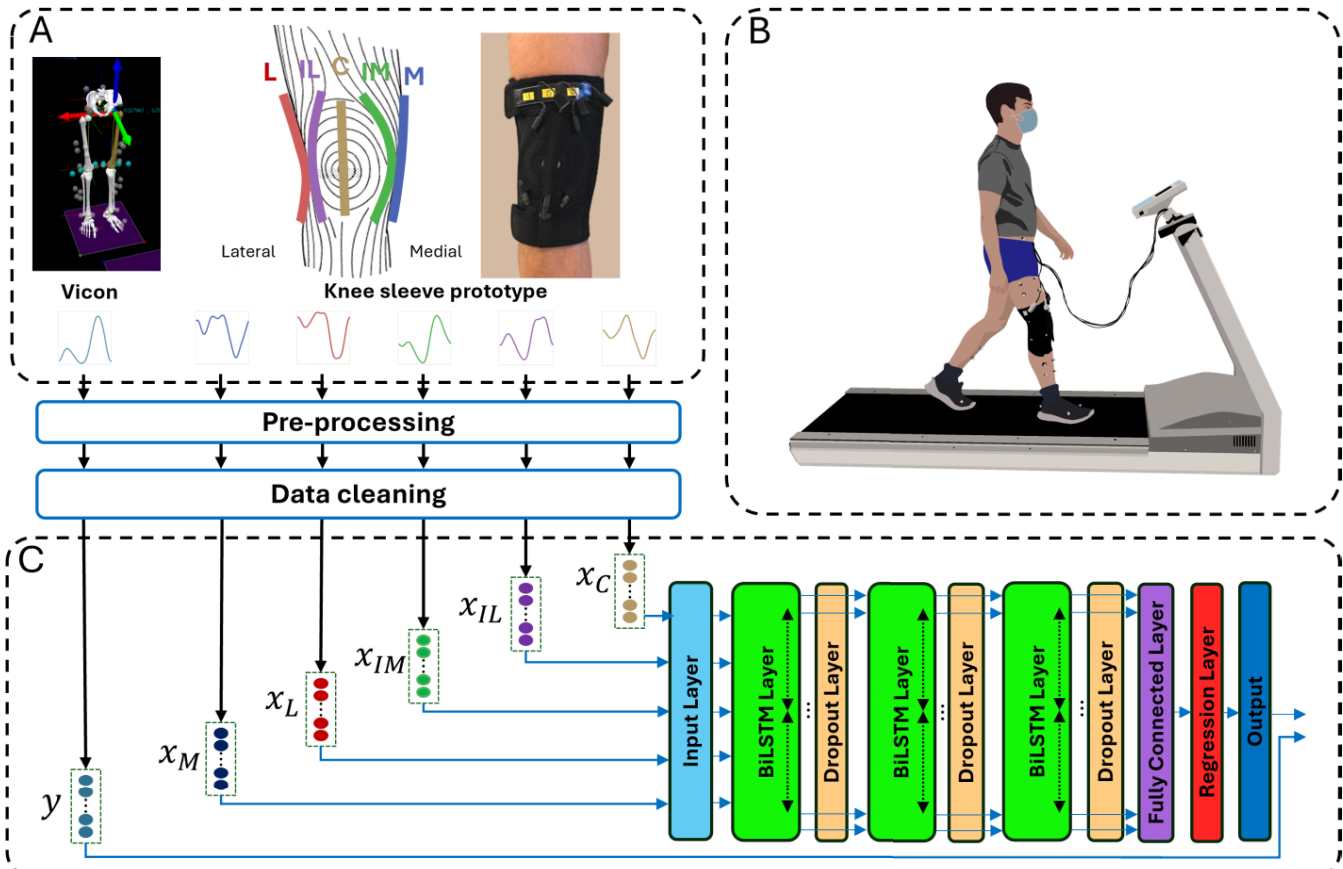
Fig. 1. Schematic representation of data acquisition and processing pipeline. A) Gold standard (camera-based motion capture system) and knee sleeve prototype; B) Experimental setup: healthy volunteer walking on a treadmill and simultaneously wearing the knee sleeve and the markers for the camera-based motion capture system; C) Data processing pipeline with a LSTM network configured for five channels. The model underwent training for various channel counts and for every possible combination for a given channel count.

Fig. 2. 3D-printed testing rig used for characterizing the multimodal POF sensor's behavior during controlled F/E movements. The optical channel is securely positioned within the rig to ensure accurate testing conditions.

attached to the rig. Data were collected using the camera-based motion capture system while flexing and extending the rig. The data were then processed in MATLAB (MathWorks, Natick, Massachusetts, USA). The sensor data were filtered with a 4th-order Butterworth low-pass filter with a 6 Hz cut-off frequency to attenuate high-frequency noise. The motion capture data were filtered with the same Butterworth filter settings. To validate the sensor's response and ensure reliable data under controlled conditions, the rig underwent multiple testing cycles. Non-linear behaviors, such as hysteresis, are expected due to the nature of the POF sensor. These non-linearities are expected to become more prominent when the sensors are integrated into the sleeve, as they must conform to the knee geometry and hence display different bending patterns during walking. These considerations suggest that a simple linear model is insufficient to capture the full range of sensor responses, thus justifying the use of an LSTM network

for further analysis due to its ability to model non-linearities and time-dependent data.

C. Experimental Acquisition

Data were collected from 31 healthy individuals (15 males; mean age: 29.2 ± 8.3 years; mean height: 173.2 ± 8.5 cm; mean weight: 69.5 ± 12.0 kg; mean body mass index: 22.7 ± 2.4 kg/m^2) while walking on a treadmill at three different speeds: self-selected (SS, 3.99 ± 0.34 km/h), fast (150% of SS), and slow (50% of SS). The choice of these three speeds was made to ensure a good representation of the variety of walking speeds and gait patterns displayed by different individuals. Thirty reflective markers were positioned on the lower limbs to collect ground truth knee F/E angle data using the motion capture system. A standard biomechanical marker set based on the calibrated anatomical landmark technique (CAST) proposed by Cappozzo et al. [34] was used. A graphic representation of a study participant during the data collection is shown in Fig. 1B.

Each participant was fitted with the appropriate size of the knee sleeve. The sleeve was calibrated using the potentiometers on the electronic circuit as described in Section II-A. All participants wore the sleeve on the right knee. Two walking trials per speed were recorded for a duration of 3 min each. The experimental procedures were approved

by the Mass General Brigham Institutional Review Board (Protocol # 2016P000424).

D. Motion Capture Data Analysis

The motion capture data were processed using the Nexus software (Vicon Motion Systems Inc, Oxford, UK). Marker trajectories were reconstructed and labeled, and gaps were filled. The processed files were then imported into Visual3D (C-Motion Inc., Germantown, Maryland, USA) that was used to implement the CAST model. The knee F/E angle, and the heel and toe markers were exported to MATLAB for further processing. The heel strike gait events were identified [35], [36], and the gait cycles were segmented from one heel strike to the next, with each segment resampled to 100 points for each gait cycle.

Outlier detection on the segmented knee F/E angles was performed using three complementary methods: (i) each gait cycle was compared to the trial mean using the Pearson correlation coefficient, with an empirically set threshold of 0.9. Gait cycles with a correlation coefficient below this value were considered abnormal and excluded; (ii) a range check was applied to detect cycles with a total ROM outside the normative range of 35° to 90° [37], ensuring that only gait-related movements were included; (iii) Dynamic Time Warping (DTW) [38] was employed to assess variations in knee F/E patterns, and cycles deviating more than three Median Absolute Deviations (MAD) from the median were considered outliers. This step was necessary to exclude data affected by measurement artifacts while preserving the natural variability of knee angles in healthy subjects. The outlier detection aimed to retain physiologically diverse but valid gait cycles, avoiding bias towards normative data. The goal was to ensure that noisy or unrepresentative cycles (e.g., due to marker gaps or heel strike identification errors) did not negatively impact the model's training and validation. Of the 27,925 total strides recorded during the study, 802 strides were considered outliers. Strides considered outliers based on the analysis of the motion capture data led to the exclusion of corresponding data across all channels.

E. Knee Sleeve Data Analysis

The output data from the five POF sensors of the knee sleeve were exported to MATLAB, where they were filtered as described in Section II-B. Following filtering, the data were segmented into strides and resampled as described above for the motion capture data.

Following the removal of outliers in a manner consistent with the motion capture system data, an additional step of outlier detection was conducted on the data collected with the POF sensors to account for aberrant sensor behaviors. One challenge in this study was the availability of only three different sleeve sizes which led to imperfect fitting for some participants. When the sleeve was not optimally fitted, migration of the sleeve during walking occurred occasionally, hence resulting in signal artifacts.

To address this issue, outlier detection on the sensor data was performed using the same multi-method approach described for the motion capture data. The Pearson correlation

coefficient threshold was set to 0.5 at this stage since abnormal gait cycles had already been excluded. This less strict criterion was applied to retain the normal variability of the signals while effectively filtering out instances where the hardware may not have functioned correctly. Gait cycles displaying a sensor output range deviating from the mean (in either the positive or negative direction) more than three times the range standard deviation were also excluded from the analysis. The DTW method was used with the same settings as described above for the motion capture data. Of the 27,123 cycles selected after removing outliers based on the motion capture data, we identified additional 2,762 aberrant gait cycles in the knee sleeve data. It should be noted that, if an outlier was detected in any channel, the corresponding data for that stride was excluded from all channels.

Signal standardization across participants presented challenges due to the variability introduced by manual calibration (as described in Section II-A) and anatomical differences. The manual adjustment of each sleeve's sensors introduced participant-specific variations, while anatomical differences across subjects affected how the sensors conformed to the knee, resulting in differences in signal dynamics. Thus, a normalization process was required.

The fast-walking trial was selected as the reference for normalization, as it displayed the largest range of motion. To assure consistency across subjects, the signal offset at a 10° knee flexion angle was removed from each channel, followed by applying the scaling factor defined in (1), calculated individually for each sensor of each participant, using the angular displacement values obtained from the motion capture

$$scaling\ factor$$
$$= \frac{percentile_{95}\left(angles\right) - percentile_5\left(angles\right)}{percentile_{95}\left(voltages\right) - percentile_5\left(voltages\right)}. \quad (1)$$

The scaling factor was derived using the 95th and 5th percentiles of the data rather than the absolute range. This method was chosen because it reduces the impact of signals with range values at the extremes of the distribution, which might not be representative of the typical sensor behavior.

F. Model Development

LSTM networks were implemented to address the expected non-linear behaviors affecting the sensors' data. The first 41 gait cycles from each of the 6 trials collected from each participant were used for model training. The processed data from the knee sleeve were used to train LSTM networks for each combination of the five sensor inputs. The segmented data were concatenated and fed to the network, with the motion capture system data serving as the ground truth.

As in previous studies that estimated knee kinematics using sensors data [26], [39], we structured the model with an input layer followed by a sequence of Bidirectional LSTM (BiLSTM) layers, each coupled with dropout layers to prevent overfitting [40]. The network architecture included a fully connected layer, and a regression layer aimed at estimating the knee F/E angle.

To optimize the model's performance, a Bayesian optimizer [41] was employed for hyperparameter tuning for

configurations with all five sensor inputs. The optimized hyperparameters were then applied to train models for all combinations of sensor inputs to enable a consistent comparison of the effect of different sensor numbers and placements, while minimizing computational cost.

The model was trained using a piecewise learning schedule, shuffling the dataset at every iteration of the dataset, for 50 iterations. The Root Mean Square Error (RMSE) per gait cycle was used as the primary performance metric. The model was evaluated using the Leave-One-Subject-Out Cross-Validation (LOSO CV) technique [42].

For each model, a Kolmogorov-Smirnov (K-S) test [43] was performed to determine if the RMSE data followed a normal distribution. This step was essential to establish the appropriate statistical method for comparing the performance of different models. Based on the non-normality of the data, the median RMSE was chosen as the primary performance metric, as it is less sensitive to outliers and better reflects typical performance across trials than the mean. The impact of the position and number of sensors on estimation accuracy was also evaluated. Various sensor configurations were tested, and their median RMSE values were compared. From these, we selected the five best-performing sensor configurations—one per sensor count—based on the lowest median RMSE values.

For the five selected configurations, a total of 38,130 RMSE data points (7,626 per sensor count) were collected across 31 participants, with each trial including 41 gait cycles and six trials per participant. Heteroscedasticity was evaluated using Levene's test [44] on the medians due to the non-normal distribution. Given the repeated measures design of the study, with 246 points per participant, the non-normal distribution, and the presence of heteroscedasticity, a rank-based mixed-effects model with heteroscedasticity-consistent standard errors (HCSE) was selected. The ranked RMSE was modeled as the dependent variable, with the five sensor combinations as the fixed effect, and participant as a random effect, accounting for the interaction between participants and sensor combinations to capture individual variability in response to each combination of sensors' data.

Post-hoc analysis was conducted using Dunn's test with Bonferroni correction [45] to explore pairwise differences between sensor configurations. To further assess the practical relevance of the differences between sensor configurations, we calculated the Common Language Effect Size (CLES) [46]. CLES provided an intuitive interpretation of the likelihood that a randomly chosen RMSE from one sensor configuration would outperform a randomly chosen RMSE from another configuration, helping to contextualize the differences in performance across sensor setups. Additionally, error distributions were analyzed across the gait cycle for the model with lowest median RMSE to evaluate performance consistency throughout the gait cycle.

III. Results

A. Sensor Characterization

The POF sensor was characterized using the above-described 3D-printed testing rig. The results shown in Fig. 3 reveal several key behaviors of the POF sensor. When we
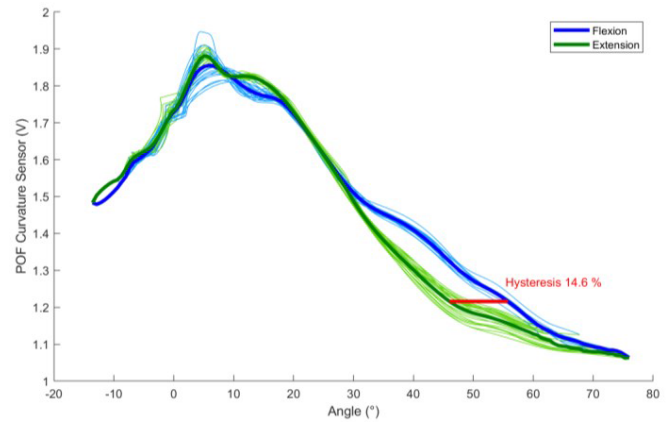

Fig. 3. Characterization of the POF bending sensor using the 3D-printed rig shown in Fig. 2. The plot displays the POF sensor output (y-axis) vs. the rig angle (x-axis). The light blue lines represent the sensor output during flexion, while the light green lines represent the sensor output during extension. The dark blue line indicates the mean flexion response, and the dark green line indicates the mean extension response. The red line marks the maximum hysteresis (i.e., 14.6%).

positioned the element of the rig at $0°$ (herein referred to as "rig angle"), the POF sensor was not straight due to the deformation induced by the shrink tubing. Hence, we observed a reduction in the transmitted light (i.e., a voltage drop compared to the position in which the sensor was straight). As the angle increased to $5°$, the POF sensor straightened, hence resulting in a peak voltage output. For rig angles above $5°$, the POF sensor began to bend, hence causing a decrease in the voltage output. A non-linear behavior was observed as the sensor bent further, likely due to a combination of changes in mode propagation and reflections within the POF sensor, along with the viscoelastic characteristics of the sensor and its conduit. These factors contributed to signal attenuation, and at bending angles greater than $30°$, the sensor's mechanical behavior led to a pronounced hysteresis effect. The maximum hysteresis was about 14.6%. These observations underscored the need for an LSTM network to model the complex, non-linear behavior exhibited by the POF sensors.

B. Data Collected

When the optical channels are integrated into the sleeve, the bending patterns become significantly more complex, as illustrated in Fig. 4. During walking, two transitions between knee F/E were observed, one occurring during the stance phase and the other during the swing phase. These transitions are most likely associated with hysteresis due to the viscoelastic properties of the sensor. Moreover, the optical channels showed a complex bending pattern when integrated into the sleeve as the sleeve conformed to the geometry of the knee in a manner that varied from subject to subject. This led to distinct bending patterns across the sensors, depending on their specific position in the sleeve. Additionally, the variations in knee geometry among different individuals introduced further complexity, resulting in unique sensor responses from person to person. These complex relationships (arising from the sleeve's design, the dynamic movements during walking,
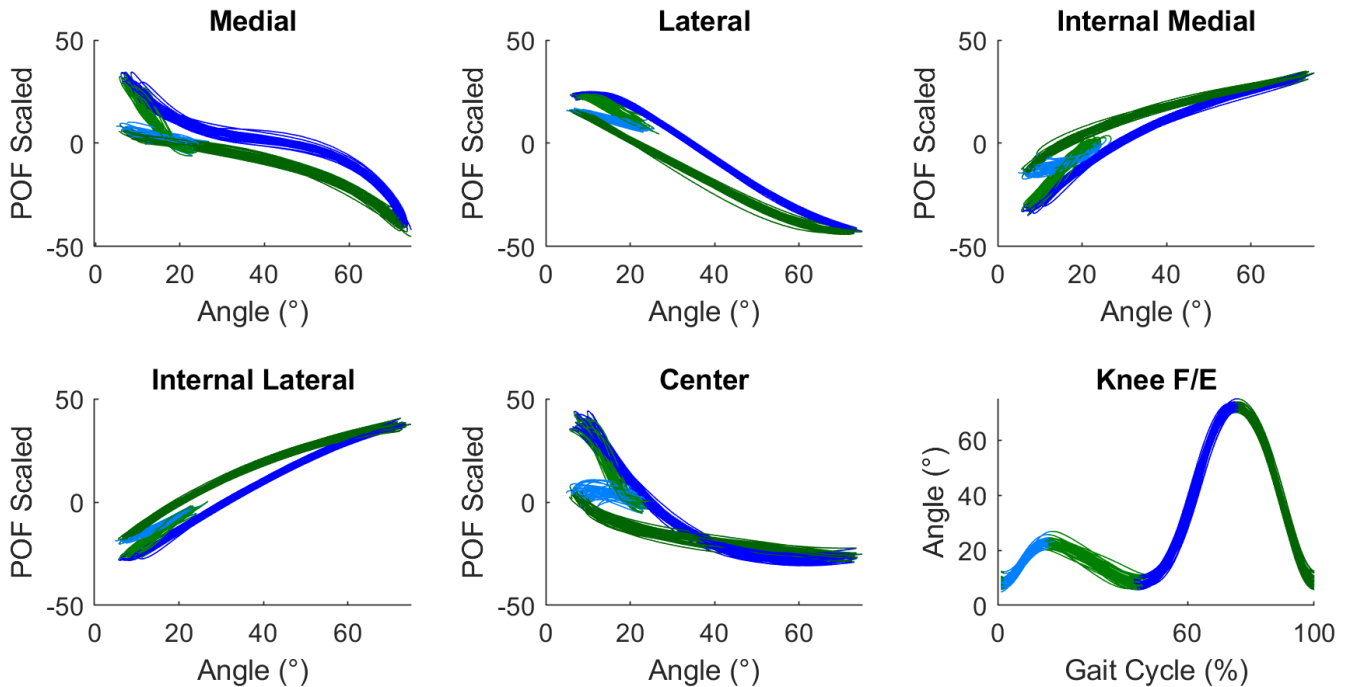
Fig. 4. Processed data from a representative participant (female, 26 years old, weight 57.5 kg, height 1.66 m) over multiple gait cycles at SS speed (4.6 km/h). The first five plots display the scaled output of the 5 optical channels (M, L, IM, IL, C) vs. the reference knee angle. The sixth plot shows the knee F/E angle versus the gait cycle percentage. The blue lines represent phases of knee flexion, while the green lines indicate phases of the knee extension.

and individual anatomical differences) provide motivation for using an LSTM network.

To complement the patterns shown in Fig. 4, Fig. 5 presents the processed outputs of the same five optical channels (M, L, IM, IL, C) across sequential gait cycles. This figure illustrates the consistency of sensor outputs over time and provides a clear view of how the sensor signals evolve across multiple gait cycles. The blue lines represent phases of knee flexion, while the green lines indicate phases of knee extension, demonstrating stable and repeatable signal patterns across gait cycles.

C. Sensors Combinations Analysis

The hyperparameters explored during the optimization process of the LSTM network with five input channels, and the optimized values applied to all sensor configurations, are reported in Table I.

The performance of various configurations of optical channels was evaluated using the RMSE across the gait cycle as the primary metric. This analysis compared the knee angle estimates derived using the LSTM model from the knee sleeve data with the ground truth motion capture data.

The results of the K-S test to assess whether each model's RMSE distribution followed a normal distribution showed non-normality across all configurations ($p < 0.001$). Given the non-normal distribution, the median RMSE and interquartile range (IQR) for each sensor configuration were reported in Fig. 6. Single-channel configurations revealed that the L

channel achieved the lowest median RMSE (3.88°, IQR: 2.85° − 5.50°). Channels IM, IL and M also showed strong performance, with a median RMSE below 4.5°, whereas the C channel had the highest error, showing the worst performance with a median RMSE exceeding 5.5°, suggesting that this channel may capture less relevant or noisier information.

Using two-channel configurations improved the performance slightly compared to single-channel setups. The combination of M and L channels performed best, yielding a median RMSE of 3.49° (IQR: 2.58° − 4.79°). Combinations such as L and IM followed closely with similar median RMSE values, while those involving the C channel performed poorly.

Three-channel setups produced the best performance with the combination of M, L, and IL achieving the lowest median RMSE of 3.41° (IQR: 2.50° − 5.19°). Combinations involving the C channel exhibited worse performance, underscoring its limited contribution in multi-channel configurations.

Four-channel configurations did not provide further improvement, with the combination of M, L, IM, and IL achieving a median RMSE of 3.53° (IQR: 2.51° − 5.22°).

The five-channel configuration produced a slightly worse performance, with a median RMSE of 3.91° (IQR: 2.60° − 5.82°), indicating that the addition of the non-optimal C channel negates the benefits observed with fewer channels.

To statistically analyze the impact of channel configurations on performance, we examined the RMSE values derived from the configuration with the lowest median RMSE for each number of channels. A Levene's test was performed showing significant heteroscedasticity ($p < 0.001$), hence supporting the use of a rank-based mixed-effects model with HCSE.
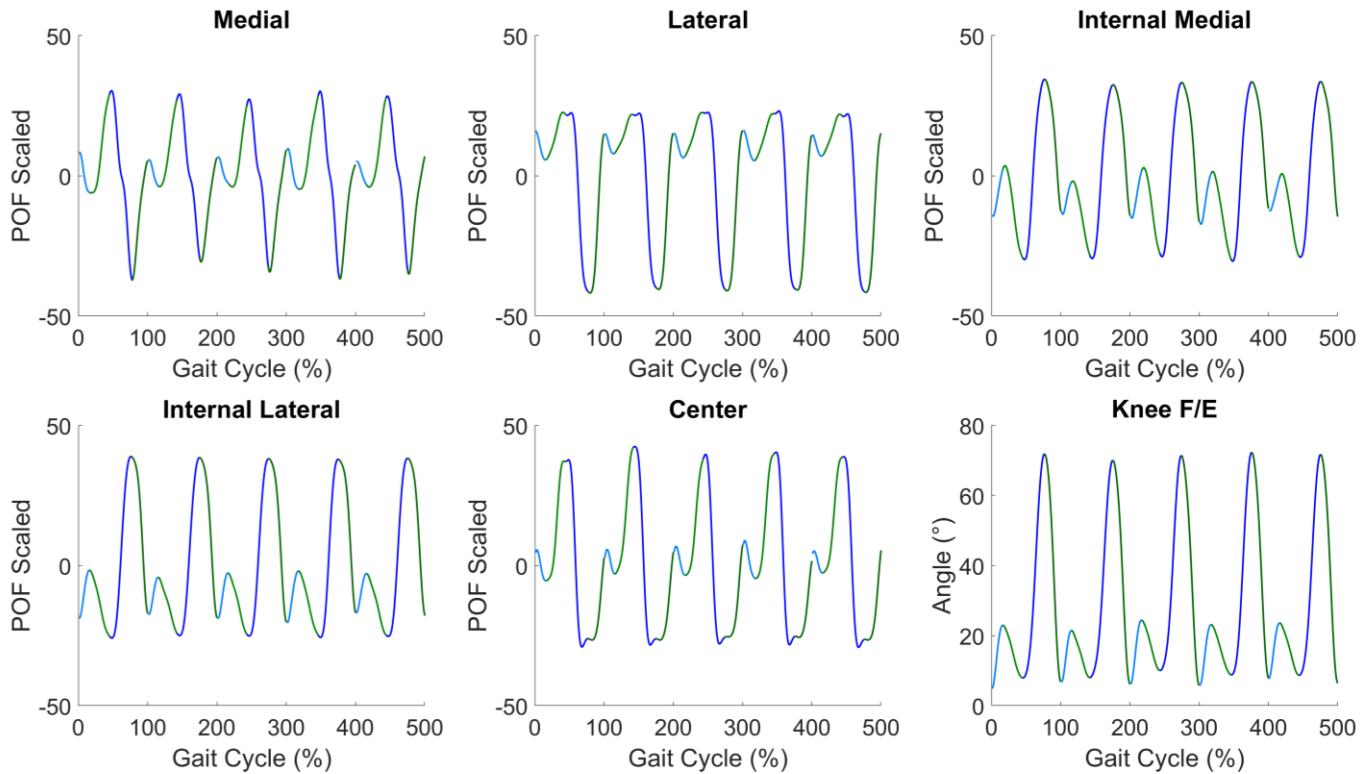
Fig. 5. Processed sensor outputs from a reference participant (female, 26 years old; weight 57.5 kg; height 1.66 m) during sequential gait cycles at SS speed (4.6 km/h). The plot displays the scaled output of the 5 optical channels (M, L, IM, IL, C) against the gait cycle percentage over multiple cycles. The blue lines represent knee flexion, while the green lines indicate knee extension.

TABLE I
HYPERPARAMETERS OPTIMIZATION

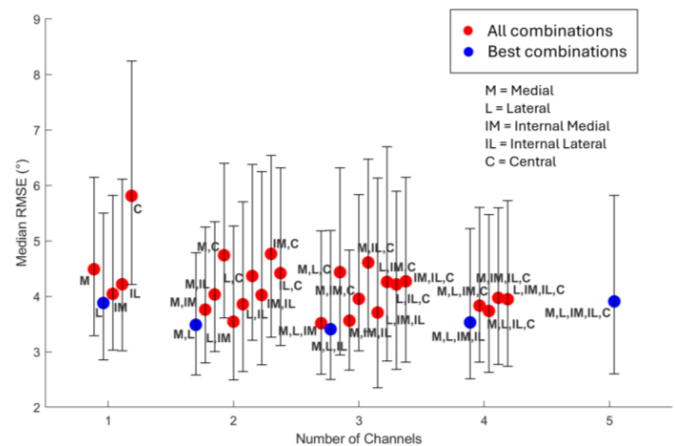| Parameter	Range	Optimized Value
#BiLSTM-Dropout layers	[1, 3]	3
#Hidden units Layer 1	[10, 250]	134
#Hidden units Layer 2	[10, 250]	26
#Hidden units Layer 3	[10, 250]	139
Dropout Factor Layer 1	[0.1, 0.5]	0.1580
Dropout Factor Layer 2	[0.1, 0.5]	0.4839
Dropout Factor Layer 3	[0.1, 0.5]	0.1283
Initial Learning Rate	[1e-4, 0.1]	0.0029
Minibatch size	[10, 256]	71
Optimizer	[adam, sgdm, rmsprop]	adam
Gradient Threshold	[0.1 10]	1.076
L2 Regularization	[1e-5, 1e-2]	3.4253e-4
Learning Rate Drop Period	[10, 50]	24
Learning Rate Drop Factor	[0.1 0.5]	0.1797

Fig. 6. Median RMSE and interquartile range (IQR) associated with different combinations of channels used to train the LSTM neural network. The x axis represents the number of channels, the y axis the RMSE error, and the label is the combination of channels. The median and IQR values were calculated across all gait cycles for each sensor configuration. The results with the lowest median RMSE are reported in blue for each number of channels considered, while all other data points are represented in red.

The ranked RMSE values were modeled as the dependent variable, with sensor combinations as a fixed effect and participants as a random effect, accounting for participant-specific variability. The rank-based mixed model demonstrated significant differences among sensor configurations ($p < 0.001$ for all channel configurations). Post-hoc pairwise comparisons using Dunn's test with Bonferroni correction revealed significant differences between several channel combinations (Table II).

Notably, the performance of the two-, three- and four-channel combinations were found to be not statistically different from each other, indicating that these configurations are likely capturing overlapping information from the knee joint. This suggests that adding more than two channels does not significantly change the quality of the information provided by the sensors. However, the performance of these configurations was found to be statistically different when

TABLE II
OUTCOMES OF DUNN'S TEST WITH BONFERRONI CORRECTION FOR
THE OPTIMAL CHANNEL COMBINATION FOR EACH
NUMBER OF CHANNELS

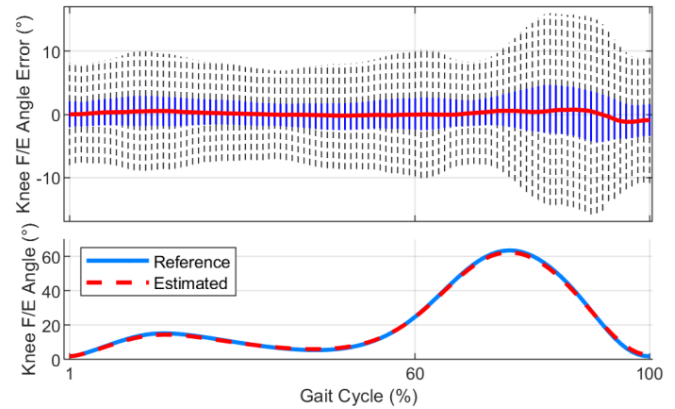| Comparison	Difference in Ranks	p-value	CLES (%)
1 vs 2	3071	< 0.001	56.2
1 vs 3	3713	< 0.001	56.5
1 vs 4	2681.5	< 0.001	55.6
1 vs 5	-189.5	< 0.001	51.8
2 vs 3	642	1	50.7
2 vs 4	-389.5	1	49.8
2 vs 5	-3260.5	< 0.001	46.3
3 vs 4	-1031.5	1	49.3
3 vs 5	-3902.5	< 0.001	46
4 vs 5	-2871	< 0.001	46.5

Fig. 7. Top: Boxplot distribution of knee angle estimation error across the gait cycle using the sensor combination with lowest median RMSE (M, L, IL) for training the LSTM neural network. Each boxplot corresponds to a percentage of the gait cycle, with whiskers set to 1.5 times the IQR. The median error was calculated for each point of the gait cycle. The red line represents the median error. Bottom: Mean knee F/E angle during the gait cycle, with the solid blue line representing the reference motion capture data, and the red dashed line indicating the estimated angles derived from the model.

compared to the single-channel and five-channel configurations. Specifically, the effect sizes calculated using CLES indicated an effect between 55.6% and 56.2% for two-, three-, and four-channel combinations compared to single-channel setups. In contrast, the effect sizes between these configurations and the five-channel setup were between 46% and 46.5%. This suggests that the single-channel setups are capturing significantly different (and more limited) information, leading to higher RMSEs, while the five-channel setup introduces a level of redundancy and noise, due to the inclusion of the C channel, which minimally worsens performance compared to the optimal two, three, and four-channel configurations.

Finally, an analysis was conducted on the best-performing three-channel configuration (M, L, IL) across different walking speeds. The results demonstrated that walking speed has a negligible impact on the system's performance, underscoring the system's reliability in diverse ambulatory conditions. Detailed results of this analysis are provided in the supplementary materials (Supplementary Section I: Repeatability Across Waking Speeds).

D. Error Distribution Across the Gait Cycle

The distribution of knee F/E angle errors across the gait cycle was derived for the combination of sensors with lowest median RMSE (M, L, IL). The top panel of Fig. 7 shows the median error and IQR values for each point of the gait cycle.

Throughout the gait cycle, the median error (represented by the red line) fluctuates around 0°, indicating that the system's estimation is generally unbiased. During the stance phase, the median error remains close to 0°, indicating minimal bias in angle estimation. During the swing phase, the median error shows a slight increase, especially during late swing. The IQR error (i.e., 25th-75th percentile error range) was between $-5°$ and $5°$. Few gait cycles exhibited larger deviations. The variability in estimation error was greater during the swing phase of the gait cycle compared to the stance phase.

The bottom panel of Fig. 7 displays the average knee F/E angle throughout the gait cycle. The blue line represents the reference motion capture data, while the dashed red line indicate the angle estimated using the sensorized sleeve. The estimated knee angle aligns well with the reference data

throughout the gait cycle, further demonstrating the accuracy of the system.

It should be noted that variability in model performance was observed across subjects. While the data for most subjects displayed RMSE values close to the optimal performance (3.41°), a few individuals exhibited larger errors, highlighting subject dependency. A detailed analysis of the RMSE distribution per subject is provided in the supplementary materials (Supplementary Section III: Impact of Interpersonal Variability).

IV. DISCUSSION

Monitoring patients with knee OA using textile-integrated sensors is appealing in the context of tracking physical activity and knee ROM to facilitate the clinical management of this condition. Wearable solutions, such as the multimodal POF bending sensors-based solution presented in this manuscript, offer a non-invasive and unobtrusive method for real-time monitoring during walking. This study demonstrates the potential of these sensors to provide valuable data for knee OA management.

The POF sensor characterization showed notable non-linearities, due to hysteresis and mode coupling. These non-linear behaviors, coupled with the cyclical nature of walking, required the use of LSTM networks for estimating knee F/E angles. The LSTM's capability to model temporal dependencies and capture sensor output complexities appeared to be critical to address these challenges, thus leading to accurate knee angle estimates.

The analysis of the error distribution during the gait cycle (Fig. 7) demonstrated that the LSTM network performed consistently well across the gait cycle, with a slight decrease in performance during the swing phase of the gait cycle. This is likely due to the rapid changes in angular displacement observed during the swing phase, which seem to amplify the non-linearities in the sensor response and hinder accurate angle

estimation. However, the estimation error was mostly limited to the range between $-5°$ and $5°$. This is compatible with clinical application of the sensorized sleeve. As a case in point, a reduction (compared to healthy controls) of approximately $8°$ in knee flexion is typically observed in patients with knee OA during the stance phase [4]. This is compatible with the system's capability to detect changes in knee angular displacement. In fact, during the stance phase, the 75th percentile error was approximately $2.90°$, well below the reduction in knee flexion that one would want to detect. Outliers showed larger error values (up to $9.96°$), hence highlighting that occasionally the performance of the knee sleeve might not be adequate.

A key factor affecting the performance of the model seemed to be related to how the sensors conform to the geometry of the knee of different individuals. We empirically observed that outliers in the error distribution were associated with subjects whose knee geometry was underrepresented in the dataset. This is further supported by the non-normal distribution and heteroscedasticity observed in the data, which highlight how different knee geometries may have led to different sensor responses and increased RMSE. This suggests that a larger, more diverse dataset, better representing different knee geometries, would enable clustering of similar geometries and the development of geometry-specific models. These personalized models would optimize estimation accuracy for each user by tailoring the system to the individual's knee geometry. Integrating biomechanical models could also enhance accuracy by adding constraints that address deviations in sensor outputs, especially for underrepresented knee geometries. Tools like OpenCap could provide the basis for implementation of these models [47].

Although this study focused on healthy participants to test the proposed sensorized knee sleeve, we are ultimately interested in using the sleeve to monitor individuals with knee OA. We recognize that patients with knee OA often exhibit altered gait patterns and greater variability in knee angles. The outlier detection process used in this study was designed to filter out noise and measurement artifacts. It may need to be adapted to accommodate for the increased variability expected in patients with knee OA. As part of future research, it will be essential to validate the system in individuals with knee OA, ensuring that the device can capture the full range of motion characteristics that mark their altered gait. This is a crucial step toward making the system robust enough for clinical use in managing OA, where real-time monitoring of knee function could aid in guiding personalized interventions.

One limitation encountered during the study was the availability of only three sleeve sizes (medium, large, and extra-large), which resulted in imperfect fitting for some participants. In cases where the sleeve did not fit snugly, we observed migration of the sleeve during walking, leading to artifacts in the sensor data. This migration altered the position of the sensors relative to the knee center of rotation, causing changes in sensor output detected as outliers and removed from the dataset. An example of this effect is provided in the supplementary materials (Supplementary Section II: Effect of Sleeve Migration on Sensor Output), which demonstrates how sleeve migration during a fast-walking trial resulted in changes in sensor output. Notably, adjusting the sleeve for a subsequent trial eliminated these artifacts and stabilized the signals. Future studies will benefit from the development of a customized (i.e. subject-specific) sleeve design to reduce the likelihood of sleeve migration and enhance signal reliability. Improving the sleeve's fit for diverse body types will be crucial to ensure consistent and accurate data collection across different users.

Using more than one sensor proved to enhance model performance. Multiple sensors placed at different anatomical locations provided complementary information, compensating for the limitations of single sensors and improving overall accuracy. However, the placement of sensors was critical, as the inclusion of the sub-optimally positioned C channel reduced performance. This finding indicates that careful consideration of sensor placement is essential, and the C channel should not be included in future configurations.

The best performance, with a median RMSE of $3.41°$ (IQR: $2.50° - 5.19°$), was achieved using three sensors. While there was no statistically significant difference between the best two-, three- and four-sensor configurations, redundancy is still recommended. Redundant sensors enhance the robustness of the system against potential sensor failures. A multiple-model approach, along with sensor failure detection logic, could be deployed. Multiple separate models for different sensor configurations could be trained and, in the event of sensor failure, an alternative model could be used to maintain high performance, even with fewer functioning sensors.

One of the challenges in deploying this device in the home and community is signal normalization across different sensor placements and users. In the study, we normalized the sensor outputs by subtracting the offset value at a $10°$ knee angle from all channels and applying a scaling factor to standardize the signal range. However, this method requires knowledge of the knee angle at $10°$ of flexion, which is impractical in real-world applications. To overcome this limitation, improvements in the electronics could be made by replacing the second (non-inverting) amplification stage with a differential amplifier. This differential amplifier would utilize a known baseline voltage, acquired during a calibration procedure when the leg is straight ($0°$), ensuring a consistent sensor output for all users. For signal range normalization, a calibration procedure with two measurement points (using sensor data when the leg is straight and at $90°$ of knee flexion) could be employed. Although this method is effective for the M and L sensors, which are pre-flexed in the sleeve, it may pose challenges for the IM and IL sensors, which are hyper-extended when the leg is straight and display a flexion pattern as the knee bends. Hence, a calibration based on capturing the sensor output at the above-mentioned two measurement points might not capture the actual full range of sensor output. An alternative solution could involve collecting sensor data over multiple gait cycles to establish the minimum and maximum sensor output, hence standardizing the sensor output without needing absolute angle information. While this would limit the ability to measure absolute angles, it would allow for the detection of relative changes in angular displacement, enabling monitoring of ROM changes, possibly associated with joint stiffening due to knee pain. We argue that the potential for real-world application

of the proposed technology is high. Although challenges remain, such as signal calibration and standardization across different users, the proposed system holds significant potential for clinical use. The system could be used for monitoring knee OA progression, guiding personalized interventions, and improving patient outcomes.

A. Limitations and Recommendations for Future Work

The data collected in this study were limited to healthy individuals, which poses questions about the generalizability of the results to individuals with knee OA, who are known to display aberrant biomechanics of knee F/E. Including OA patients in future datasets would be key to improve the model's robustness for clinical use.

Only three sleeve sizes were available, which resulted occasionally in poor fitting and sleeve migration, thus introducing signal artifacts. Developing customized sleeve designs could mitigate these issues by ensuring a better fit across different anatomical profiles. To further reduce the impact of migration artifacts, implementing a quality-check algorithm that monitors signal consistency and detects deviations indicative of sleeve movement is recommended.

Higher errors observed in a subset of participants suggest that underrepresented knee geometries in the dataset may contribute to inaccuracies. Collecting a larger and more anatomically diverse dataset could address this limitation. By clustering anatomical characteristics, geometry-specific models could be developed to enhance system accuracy for individuals with varied knee shapes.

The system's repeatability under donning and doffing conditions was not evaluated. Future studies should include tests collecting data by instructing subjects to don/doff the sleeve hence incorporating variability in the training set to enhance the model's robustness to variations associated with donning and doffing the sleeve.

Lastly, the sensor signal normalization method used in the study, reliant on a controlled calibration (i.e., using data collected for a specific knee angle), may pose challenges in home deployments. Alternative methods have been proposed and warrant further exploration to enable robust performance in real-world environments.

Addressing these limitations will enhance the reliability and applicability of the proposed system in clinical, real-world scenarios.

V. CONCLUSION

This study highlights the potential of integrating multimodal POF bending sensors into a wearable knee sleeve for real-time monitoring of knee F/E patterns. We showed that the use of LSTM networks effectively addresses the non-linearities affecting the sensors' output when they are integrated into a knee sleeve. The results show that sensor redundancy improves estimation accuracy, with a three-channel configuration providing the best performance. The device shows promise for real-world applications in monitoring the biomechanics of patients with knee OA. Future work should focus on enhancing sensor calibration methods and expanding datasets to improve the accuracy of the system for different knee geometries.

REFERENCES

[1] E. N. Ringdahl, "Treatment of knee osteoarthritis," *Amer. Family Physician*, vol. 83, no. 11, pp. 1287–1292, Jun. 2011.

[2] K. R. Kaufman, C. Hughes, B. F. Morrey, M. Morrey, and K.-N. An, "Gait characteristics of patients with knee osteoarthritis," *J. Biomech.*, vol. 34, no. 7, pp. 907–915, Jul. 2001, doi: 10.1016/S0021-9290(01)00036-7.

[3] J. D. Childs, P. J. Sparto, G. K. Fitzgerald, M. Bizzini, and J. J. Irrgang, "Alterations in lower extremity movement and muscle activation patterns in individuals with knee osteoarthritis," *Clin. Biomech.*, vol. 19, no. 1, pp. 44–49, Jan. 2004, doi: 10.1016/j.clinbiomech.2003.08.007.

[4] I. McCarthy, D. Hodgins, A. Mor, A. Elbaz, and G. Segal, "Analysis of knee flexion characteristics and how they alter with the onset of knee osteoarthritis: A case control study," *BMC Musculoskeletal Disorders*, vol. 14, no. 1, p. 169, Dec. 2013, doi: 10.1186/1471-2474-14-169.

[5] S. Farrokhi, M. O'Connell, and G. K. Fitzgerald, "Altered gait biomechanics and increased knee-specific impairments in patients with coexisting tibiofemoral and patellofemoral osteoarthritis," *Gait Posture*, vol. 41, no. 1, pp. 81–85, Jan. 2015, doi: 10.1016/j.gaitpost.2014.08.014.

[6] K. Bennell and R. Hinman, "Exercise as a treatment for osteoarthritis," *Current Opinion Rheumatology*, vol. 17, no. 5, pp. 634–640, Sep. 2005, doi: 10.1097/01.bor.0000171214.49876.38.

[7] N. J. Bosomworth, "Exercise and knee osteoarthritis: Benefit or hazard?" *Can. Family Physician*, vol. 55, no. 9, pp. 871–878, Sep. 2009.

[8] M. Fransen, S. McConnell, A. R. Harmer, M. Van der Esch, M. Simic, and K. L. Bennell, "Exercise for osteoarthritis of the knee: A cochrane systematic review," *Brit. J. Sports Med.*, vol. 49, no. 24, pp. 1554–1557, Dec. 2015, doi: 10.1136/bjsports-2015-095424.

[9] K. M. Leyland et al., "Measuring the variation between self-reported osteoarthritis pain assessments," *Osteoarthritis Cartilage*, vol. 24, p. S8, Apr. 2016, doi: 10.1016/j.joca.2016.01.044.

[10] P. W. Stratford, D. M. Kennedy, and L. J. Woodhouse, "Performance measures provide assessments of pain and function in people with advanced osteoarthritis of the hip or knee," *Phys. Therapy*, vol. 86, no. 11, pp. 1489–1496, Nov. 2006, doi: 10.2522/ptj.20060002.

[11] P. Bonato, V. Feipel, G. Corniani, G. Arin-Bal, and A. Leardini, "Position paper on how technology for human motion analysis and relevant clinical applications have evolved over the past decades: Striking a balance between accuracy and convenience," *Gait Posture*, vol. 113, pp. 191–203, Sep. 2024, doi: 10.1016/j.gaitpost.2024.06.007.

[12] A. I. Faisal, S. Majumder, T. Mondal, D. Cowan, S. Naseh, and M. J. Deen, "Monitoring methods of human body joints: State-of-the-art and research challenges," *Sensors*, vol. 19, no. 11, p. 2629, Jun. 2019, doi: 10.3390/s19112629.

[13] S. Prachi, A. Rohit Kumar, P. Suraj, and S. Mandeep, "Fibre optic Communications: An overview," *Int. J. Emerg. Technol. Adv. Eng.*, vol. 3, no. 5, pp. 474–479, May 2013.

[14] K. Peters, "Polymer optical fiber sensors—A review," *Smart Mater. Struct.*, vol. 20, no. 1, Jan. 2011, Art. no. 013002, doi: 10.1088/0964-1726/20/1/013002.

[15] K. Cherenack and L. Van Pieterson, "Smart textiles: Challenges and opportunities," *J. Appl. Phys.*, vol. 112, no. 9, Nov. 2012, Art. no. 091301, doi: 10.1063/1.4742728.

[16] M. Gholami, A. Rezaei, T. J. Cuthbert, C. Napier, and C. Menon, "Lower body kinematics monitoring in running using fabric-based wearable sensors and deep convolutional neural networks," *Sensors*, vol. 19, no. 23, p. 5325, Dec. 2019, doi: 10.3390/s19235325.

[17] L. Bilro, J. G. Oliveira, J. L. Pinto, and R. N. Nogueira, "A reliable low-cost wireless and wearable gait monitoring system based on a plastic optical fibre sensor," *Meas. Sci. Technol.*, vol. 22, no. 4, Apr. 2011, Art. no. 045801, doi: 10.1088/0957-0233/22/4/045801.

[18] D. A. B. Miller, "Waves, modes, communications, and optics: A tutorial," *Adv. Opt. Photon.*, vol. 11, no. 3, p. 679, Sep. 2019, doi: 10.1364/aop.11.000679.

[19] J. M. Kahn, K.-P. Ho, and M. B. Shemirani, "Mode coupling effects in multi-mode fibers," in *Proc. Opt. Fiber Commun. Conf.*, Los Angeles, CA, USA, Mar. 2012, pp. 1–3, doi: 10.1364/OFC.2012.OW3D.3.

[20] A. G. Leal-Junior, A. Frizera-Neto, M. J. Pontes, and T. R. Botelho, "Hysteresis compensation technique applied to polymer optical fiber curvature sensor for lower limb exoskeletons," *Meas. Sci. Technol.*, vol. 28, no. 12, Dec. 2017, Art. no. 125103, doi: 10.1088/1361-6501/aa946f.

[21] H. Sepp and S. Jürgen, "Long short-term memory," *Neural Comput.*, vol. 9, no. 8, pp. 1735–1780, 1997, doi: 10.1162/neco.1997.9.8.1735.

[22] M. T. N. Truong, A. E. A. Ali, D. Owaki, and M. Hayashibe, "EMG-based estimation of lower limb joint angles and moments using long short-term memory network," *Sensors*, vol. 23, no. 6, p. 3331, Mar. 2023, doi: 10.3390/s23063331.

[23] R. D. Gurchiek, N. Cheney, and R. S. McGinnis, "Estimating biomechanical time-series with wearable sensors: A systematic review of machine learning techniques," *Sensors*, vol. 19, no. 23, p. 5227, Nov. 2019, doi: 10.3390/s19235227.

[24] T. T. Alemayoh, J. H. Lee, and S. Okamoto, "Leg-joint angle estimation from a single inertial sensor attached to various lower-body links during walking motion," *Appl. Sci.*, vol. 13, no. 8, p. 4794, Apr. 2023, doi: 10.3390/app13084794.

[25] L. Tong, R. Liu, and L. Peng, "LSTM-based lower limbs motion reconstruction using low-dimensional input of inertial motion capture system," *IEEE Sensors J.*, vol. 20, no. 7, pp. 3667–3677, Apr. 2020, doi: 10.1109/JSEN.2019.2959639.

[26] J.-S. Tan et al., "Predicting knee joint kinematics from wearable sensor data in people with knee osteoarthritis and clinical considerations for future machine learning models," *Sensors*, vol. 22, no. 2, p. 446, Jan. 2022, doi: 10.3390/s22020446.

[27] J. Sung et al., "Prediction of lower extremity multi-joint angles during overground walking by using a single IMU with a low frequency based on an LSTM recurrent neural network," *Sensors*, vol. 22, no. 1, p. 53, Dec. 2021, doi: 10.3390/s22010053.

[28] D. D. Molinaro, I. Kang, J. Camargo, M. C. Gombolay, and A. J. Young, "Subject-independent, biological hip moment estimation during multimodal overground ambulation using deep learning," *IEEE Trans. Med. Robot. Bionics*, vol. 4, no. 1, pp. 219–229, Feb. 2022, doi: 10.1109/TMRB.2022.3144025.

[29] K. Langer, "On the anatomy and physiology of the skin. I. The cleavability of the cutis," *Brit. J. Plastic Surg.*, vol. 31, no. 1, pp. 3–8, Jan. 1978.

[30] K. Langer, "On the anatomy and physiology of the skin. II. Skin tension," *Brit. J. Plastic Surg.*, vol. 31, no. 2, pp. 93–106, Apr. 1978.

[31] K. Langer, "On the anatomy and physiology of the skin. III. The elasticity of the cutis," *Brit. J. Plastic Surg.*, vol. 31, no. 3, pp. 185–199, Jul. 1978.

[32] K. Langer, "On the anatomy and physiology of the skin. IV. The swelling capabilities of skin," *Brit. J. Plastic Surg.*, vol. 31, no. 4, pp. 273–276, Oct. 1978.

[33] K. Langer, "On the anatomy and physiology of the skin: Conclusions," *Brit. J. Plastic Surg.*, vol. 31, no. 4, pp. 277–278, Oct. 1978, doi: 10.1016/s0007-1226(78)90109-1.

[34] A. Cappozzo, F. Catani, U. D. Croce, and A. Leardini, "Position and orientation in space of bones during movement: Anatomical frame definition and determination," *Clin. Biomech.*, vol. 10, no. 4, pp. 171–178, Jun. 1995, doi: 10.1016/0268-0033(95)91394-T.

[35] S. Ghoussayni, C. Stevens, S. Durham, and D. Ewins, "Assessment and validation of a simple automated method for the detection of gait events and intervals," *Gait Posture*, vol. 20, no. 3, pp. 266–272, Dec. 2004, doi: 10.1016/j.gaitpost.2003.10.001.

[36] J. A. Zeni, J. G. Richards, and J. S. Higginson, "Two simple methods for determining gait events during treadmill and overground walking using kinematic data," *Gait Posture*, vol. 27, no. 4, pp. 710–714, May 2008, doi: 10.1016/j.gaitpost.2007.07.007.

[37] J. R. Brinkmann and J. Perry, "Rate and range of knee motion during ambulation in healthy and arthritic subjects," *Phys. Therapy*, vol. 65, no. 7, pp. 1055–1060, Jul. 1985, doi: 10.1093/ptj/65.7.1055.

[38] D. J. Berndt and J. Clifford, "Using dynamic time warping to find patterns in time series," in *Proc. 3rd Int. Conf. Knowl. Discovery Data Mining*, Jul. 1994, pp. 359–370.

[39] D. Hollinger, M. Schall, H. Chen, S. Bass, and M. Zabala, "The influence of gait phase on predicting lower-limb joint angles," *IEEE Trans. Med. Robot. Bionics*, vol. 5, no. 2, pp. 343–352, May 2023, doi: 10.1109/TMRB.2023.3260261.

[40] N. Srivastava, G. Hinton, A. Krizhevsky, I. Sutskever, and R. Salakhutdinov, "Dropout: A simple way to prevent neural networks from overfitting," *J. Mach. Learn. Res.*, vol. 15, no. 1, pp. 1929–1958, Jan. 2014.

[41] R. Martinez-Cantin, "BayesOpt: A Bayesian optimization library for nonlinear optimization, experimental design and bandits," *J. Mach. Learn. Res.*, vol. 15, no. 1, pp. 3735–3739, Nov. 2014.

[42] D. Gholamiangonabadi, N. Kiselov, and K. Grolinger, "Deep neural networks for human activity recognition with wearable sensors: Leave-one-subject-out cross-validation for model selection," *IEEE Access*, vol. 8, pp. 133982–133994, 2020, doi: 10.1109/ACCESS.2020.3010715.

[43] H. W. Lilliefors, "On the kolmogorov–Smirnov test for normality with mean and variance unknown," *J. Amer. Stat. Assoc.*, vol. 62, no. 318, pp. 399–402, Jun. 1967, doi: 10.1080/01621459.1967.10482916.

[44] R. J. Carroll and H. Schneider, "A note on levene's tests for equality of variances," *Statist. Probab. Lett.*, vol. 3, no. 4, pp. 191–194, Jul. 1985, doi: 10.1016/0167-7152(85)90016-1.

[45] A. Dinno, "Nonparametric pairwise multiple comparisons in independent groups using dunn's test," *Stata J., Promoting Commun. Statist. Stata*, vol. 15, no. 1, pp. 292–300, Apr. 2015, doi: 10.1177/1536867X1501500117.

[46] K. O. McGraw and S. P. Wong, "A common language effect size statistic," *Psychol. Bull.*, vol. 111, no. 2, pp. 361–365, 1992.

[47] S. D. Uhlrich et al., "OpenCap: Human movement dynamics from smartphone videos," *PLOS Comput. Biol.*, vol. 19, no. 10, Oct. 2023, Art. no. e1011462, doi: 10.1371/journal.pcbi.1011462.